

Learnable Locality-Sensitive Hashing for Video Anomaly Detection

Yue Lu *

Congqi Cao ^{*,†}

Yanning Zhang

School of Computer Science, Northwestern Polytechnical University
zugexiaodui@mail.nwpu.edu.cn, {congqi.cao, ynzhang}@nwpu.edu.cn

Abstract

Video anomaly detection (VAD) mainly refers to identifying anomalous events that have not occurred in the training set where only normal samples are available. Existing works usually formulate VAD as a reconstruction or prediction problem. However, the adaptability and scalability of these methods are limited. In this paper, we propose a novel distance-based VAD method to take advantage of all the available normal data efficiently and flexibly. In our method, the smaller the distance between a testing sample and normal samples, the higher the probability that the testing sample is normal. Specifically, we propose to use locality-sensitive hashing (LSH) to map samples whose similarity exceeds a certain threshold into the same bucket in advance. In this manner, the complexity of near neighbor search is cut down significantly. To make the samples that are semantically similar get closer and samples not similar get further apart, we propose a novel learnable version of LSH that embeds LSH into a neural network and optimizes the hash functions with contrastive learning strategy. The proposed method is robust to data imbalance and can handle the large intra-class variations in normal data flexibly. Besides, it has a good ability of scalability. Extensive experiments demonstrate the superiority of our method, which achieves new state-of-the-art results on VAD benchmarks.

1. Introduction

Video anomaly detection (VAD) aims to identify anomalous events that do not conform to the expectation, where typically only normal samples are available during training [34]. It plays an important role in intelligent surveillance. However, it is a highly challenging task for the following reasons. First, anomalous events are defined according to circumstances, thus the same activity may be normal or anomalous in different scenes. Second, traditional su-

pervised binary-classification methods are inapplicable to VAD, due to the absence of anomalous events in training set [23, 24, 36]. Third, some kinds of normal events happen frequently while some happen occasionally. Therefore, diverse training data has large intra-class variations and imbalanced distribution.

Prevalent VAD methods can be classified into distance-based, reconstruction-based and prediction-based methods. Distance-based methods detect anomalies according to the distance between testing data and representations of all the normal data. Representative methods are based on video patches [33, 35], decision boundaries of one-class SVM [15, 16] and cluster centers [4, 26, 40]. However, these existing methods are not adaptive enough since some essential settings (e.g. the number of clusters) are determined artificially. Besides, they suffer from large computation cost. Reconstruction-based methods [1, 7, 12, 13, 28] and prediction-based methods [2, 10, 17, 21, 22, 25, 27, 30, 36] train auto-encoders on normal data to reconstruct the current frame or to predict the next frame. They assume that anomalous frames are hard to reconstruct or predict, hence anomalies can be detected according to high reconstruction or prediction errors. The main drawback of these methods is that they do not consider the diversity of normal patterns explicitly [30]. Hence, the adaptability and scalability of these methods to complex scenarios are limited. To tackle this problem, a number of recent works augment reconstruction-based or prediction-based methods with distance-based methods, such as [12], [30], [25], [2] and [22]. Concretely, they design a memory module to store prototypical normal patterns in training phase and retrieve them in testing phase for reconstruction or prediction.

Considering the challenges of VAD, there is no sufficient and valid supervision knowledge in training phase to direct us what information we could discard. We intend to make full use of all the normal data for video anomaly detection. Therefore, in this paper, we propose an efficient distance-based method, named Learnable Locality-Sensitive Hashing (LLSH), to distinguish anomalies from normal events. Instead of directly comparing the distance

*Equal contribution.

†Corresponding author.

between the testing sample and every training sample which would bring huge computational cost, we propose to use locality-sensitive hashing (LSH) to hash normal samples into buckets in advance, where samples whose similarity exceeds an approximate threshold are mapped into the same bucket. During anomaly detection, the testing sample is also mapped into a bucket. We only need to compute the distance between the testing sample and normal samples in the same bucket. As a result, the complexity of near neighbor search is cut down significantly. Given that the representations of data are normally high-dimensional, we propose to compute the distances between low-dimensional hash codes instead of the original representations, which further reduces the computation cost. Vanilla LSH uses random vectors in hash functions, which limits its adaptability for target datasets. To make the samples that are semantically similar get closer and samples not similar get further apart according to the known data structure, we propose a novel learnable locality-sensitive hashing (LLSH). It implements LSH as a parametric network layer and embeds it into an end-to-end trainable neural network. Due to lack of explicit supervision information, we propose to optimize LLSH using contrastive learning strategy, where MoCo [14] is adopted in our framework. Our proposed LLSH is shown in Fig. 1. The architecture contains two symmetric parts. Each part is composed of a pre-trained CNN for feature extraction and a hash encoder. There is a set of parallel hash layers in the hash encoder to map the features to low-dimensional hash codes. For contrastive learning, video snippets are fed into the symmetric network simultaneously. A queue is maintained in the right part to calculate *InfoNCE* loss among the hash codes stored in it and the current hash code output by the left part. The parameters in the left part are updated through back-propagation, while those in the right part are updated by momentum. After the optimization, the hash functions in the hash layers are tuned to be more adaptive to target datasets, hence improving the performance for VAD.

Our proposed LLSH can be regarded as an advanced version of KNN, which adaptively sets the number of nearest neighbors according to similarity thresholds. In LLSH, a bucket is actually a cluster of similar samples. Therefore, it also can be seen as an advanced version of K-means, where the number of clusters (*i.e.* buckets) are adaptively determined by the distribution of normal data. In addition to the superior of adaptability, LLSH is much more efficient compared with KNN and K-means. Its computation cost is only 0.26% of KNN and 3.00% of K-means in our experiments. Compared with memory modules, LLSH retains the whole knowledge of training data. Hence, it is robust to data imbalance and can handle the large intra-class variations in normal data flexibility, which outperforms recent memory-augmented prediction methods by 4% \sim 7% in experiments. Besides, LLSH has a good ability of scala-

bility for newly added data, leading competing methods by 2% \sim 6%.

We conduct extensive experiments on three VAD benchmarks, *i.e.*, Avenue [23], ShanghaiTech [24] and Corridor [36] datasets. Our proposed LLSH achieves new state-of-the-art results on the three datasets in both micro-AUC and macro-AUC metrics. Especially for the datasets with complex scenarios, our method surpasses existing methods with a large margin. The efficiency, adaptability and scalability of LLSH are fully verified. Our code is available at <https://github.com/zugexiaodui/LLSHforVAD>.

In summary, our main contributions include:

- We introduce locality-sensitive hashing (LSH) and develop its paradigm of calculating distance for video anomaly detection.
- We propose a learnable locality-sensitive hashing (LLSH) that embeds LSH in an end-to-end trainable neural network and tunes the hash functions automatically in a contrastive learning framework.
- Our proposed LLSH is superior in efficiency, adaptability and scalability, achieving new state-of-the-art performance on VAD datasets.

2. Related Work

Distance-based Video Anomaly Detection. Distance-based methods create a model to learn the representations of normal data, and measure deviations from the model to determine anomaly scores. Video patches [33, 35], decision boundaries of one-class SVM [15, 16, 37, 38, 41] and cluster centers [4, 26, 40] are commonly used in distance-based methods. For example, Ramachandra *et al.* [35] build a concise representative exemplar set of normal video patches to reduce the number of training samples. They employ a simple nearest neighbor lookup for anomaly detection. Wang *et al.* [40] train a deep k -cluster model for normal data, and detect the anomaly by the similarities between its representations and corresponding k centers. Compared with the above methods, our proposed LLSH takes full advantage of the knowledge of normal data. It has a stronger ability of adaptability to flexibly handle the large intra-class variations in normal data.

Deep Hashing. Deep hashing is a combination of deep learning and hashing algorithms. In the field of computer vision, it is widely used in image retrieval, such as [19], [20] and [29]. They aim to produce similar binary codes for semantically similar data, which is the same as the motivation of our learning process. However, VAD is more challenging since there is no supervision information. We tackle this problem by contrastive learning strategy.

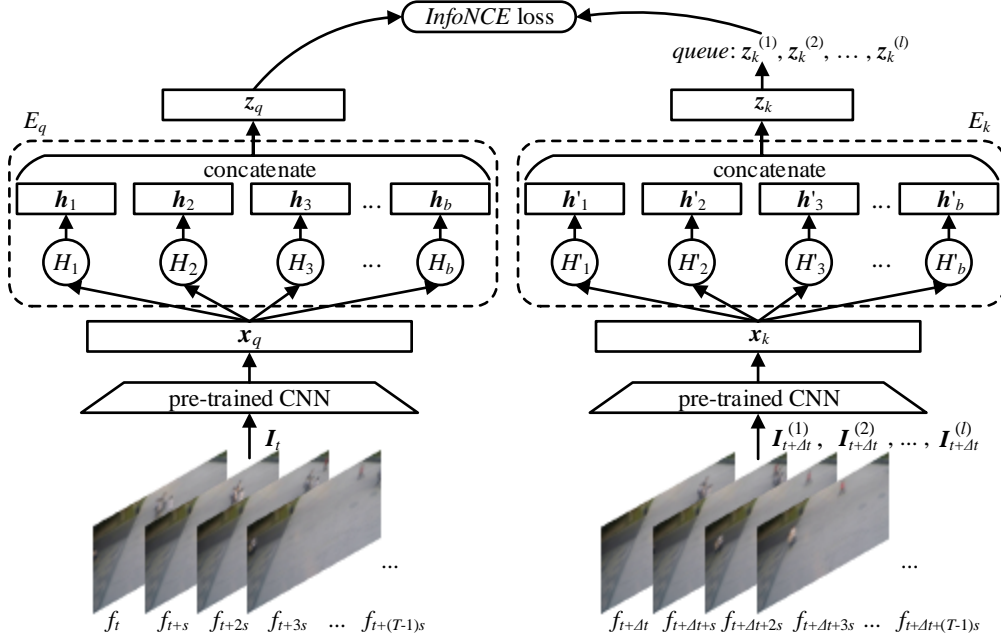


Figure 1. Overview of the proposed learnable locality-sensitive hashing. The architecture is divided into two symmetric parts. For each part, a pre-trained CNN extracts a feature \boldsymbol{x} of the sampled video snippet \boldsymbol{I} at first. Then, \boldsymbol{x} is fed into an encoder E and generates a low-dimensional hash code \boldsymbol{z} . The encoder is composed of b parallel hash layers. A total of l \boldsymbol{z}_k s are put in a queue to participate in the calculation of *InfoNCE* loss with \boldsymbol{z}_q .

Contrastive Learning. In self-supervised learning, contrastive learning approaches (e.g. SimCLR [5], MoCo [14]) present promising performance for image representations. They use contrastive loss functions to narrow the distance between a positive pair of transformed inputs from the same sample, and broaden the distances of negative pairs from different samples. Feichtenhofer *et al.* [9] propose that temporally-persistent features in the same video are effective for video representations, which inspires the design of LLSH. In VAD, Wang *et al.* [40] adopt MoCo to drive the deep clustering. They use several spatial transformations for the same snippet to generate positive pairs, but ignore the temporal relations of different snippets. We use temporally nearby snippets as positive pairs, which is simpler and more efficient in practice.

3. Method

3.1. Learnable Hashing

In the training phase, we aim to train a hashing network that encodes video snippets to short hash codes. An overview of our learnable locality-sensitive hashing (LLSH) is shown in Fig. 1. The left and right parts of the model have symmetric structures.

For the left part, firstly, a total of T frames starting from the t -th frame are sampled as a video snippet \boldsymbol{I}_t with a sampling-rate s . Next, the snippet \boldsymbol{I}_t is fed into a pre-

trained CNN to extract a feature vector \boldsymbol{x}_q . Then, we take \boldsymbol{x}_q as the input of the hash encoder E_q , which contains b parallel hash layers H_1, H_2, \dots, H_b . In our implementation, they are fully-connected layers with *sigmoid* function. Note that these fully-connected layers do not have bias terms. Each layer $H_i, i \in \{1, 2, \dots, b\}$, maps \boldsymbol{x}_q to a short hash code \boldsymbol{h}_i of length r . Every bit of \boldsymbol{h}_i gets a value in the range of $(0, 1)$ because of the *sigmoid* function. All the b short hash codes are concatenated as a long code \boldsymbol{z}_q to participate in the calculation of loss.

The right part is symmetrical to the left and uses the same initialization. A snippet $\boldsymbol{I}_{t+\Delta t}$, in which Δt is a temporal offset, is sampled as the input for the right part. The recent l codes $\boldsymbol{z}_k^{(1)}, \boldsymbol{z}_k^{(2)}, \dots, \boldsymbol{z}_k^{(l)}$ output by E_k are put in a first-in-first-out (FIFO) queue. Finally, we compute the *InfoNCE* loss [39] between \boldsymbol{z}_q and the hash codes in the queue:

$$L = -\log \frac{\exp(\boldsymbol{z}_q \cdot \boldsymbol{z}_{k+} / \tau)}{\sum_{i=0}^l \exp(\boldsymbol{z}_q \cdot \boldsymbol{z}_k^{(i)} / \tau)}, \quad (1)$$

where \boldsymbol{z}_{k+} is the one output at the same time with \boldsymbol{z}_q , and τ is a temperature hyper-parameter,

In the back-propagation phase, only the parameters θ_q of E_q are updated. The parameters θ_k of E_k is updated by momentum [14]:

$$\theta_k \leftarrow m\theta_k + (1 - m)\theta_q, \quad (2)$$

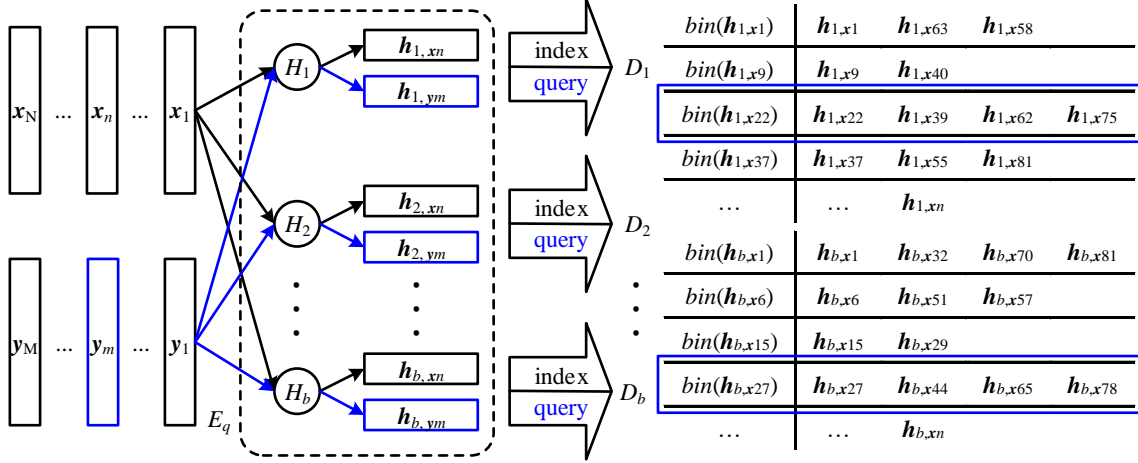


Figure 2. Overview of our anomaly detection, which includes two sequential stages: index and query. In the index stage, the hash codes of training features x_1, \dots, x_N are stored in b parallel hash tables D_1, \dots, D_b . In the query stage (in blue color), every testing feature y_i ($i \in \{1, \dots, M\}$) finds b sets of similar hash codes.

where $m \in [0, 1]$ is a momentum coefficient. The parameters of the pre-trained CNN are frozen.

Via the above operations, the hashing process is transformed into a parametric and differentiable operation that can be embedded into neural networks and trained end-to-end with contrastive learning strategy. We can get hash functions that are more adaptive to data distribution and perform anomaly detection based on it.

3.2. Anomaly Detection

In the anomaly detection phase, we aim to calculate the distances between the representations of a testing sample and its similar training samples. To this end, we propose to use the optimized locality-sensitive hashing to search similar items.

The process of our anomaly detection includes an index stage and a query stage. Only the left part of the model after training is used in both stages. In the index stage, all hash codes of training data are stored in hash tables. In the query stage, for each hash code of testing data, similar hash codes of training data are looked up from the hash tables. The anomaly score is determined by their distances. An illustration of the anomaly detection process is shown in Fig. 2.

3.2.1 Index

The features of training data extracted by the pre-trained CNN are denoted as x_1, \dots, x_N , where N represents the number of training samples. First, The n -th feature x_n ($n \in \{1, \dots, N\}$) is mapped to b hash codes of r bits $h_{1,x_n}, \dots, h_{b,x_n}$ by the parallel hash layers H_1, \dots, H_b in E_q . Next, we construct b hash tables to store the representations

(i.e. hash codes) of x_1, \dots, x_N .

We use $bin(\cdot) \in \{0, 1\}^r$ to denote the binary function:

$$bin(\mathbf{h}) = \begin{cases} 1, & \text{if } \mathbf{h}^{<i>} \geq 0.5, \\ 0, & \text{if } \mathbf{h}^{<i>} < 0.5, \end{cases} \quad \text{for all } i \in \{1, \dots, r\}. \quad (3)$$

In the j -th hash table D_j ($j \in \{1, \dots, b\}$), for all $n \in \{1, \dots, N\}$, h_{j,x_n} and its binary code $bin(h_{j,x_n})$ are respectively stored as a value and a key. The values sharing the same key are stored in the same bucket. As a result, each hash table stores N hash codes with a number of binary-valued keys.

3.2.2 Query

The features of testing data are denoted as y_1, \dots, y_M , where M represents the number of testing samples. We take the m -th ($m \in \{1, \dots, M\}$) feature y_m for example to demonstrate the process and principle of our query stage. First, it is also mapped to b hash codes $h_{1,y_m}, \dots, h_{b,y_m}$ by the hash layers. We use the binary code $bin(h_{j,y_m})$ as the key to look up a bucket in D_j , $j \in \{1, \dots, b\}$. For example, in Fig. 2, the blue box of D_1 represents the bucket of h_{1,y_m} . Since the hash codes of the training data stored in this bucket are similar to h_{1,y_m} , their original features are treated as similar candidates of y_m .

For simplicity, suppose that H_j is a stack of r random vectors. Thus, the i -th ($i \in \{1, \dots, r\}$) bit of h_{j,y_m} is a dot product of the i -th random vector in H_j and y_m . Suppose a training vector x_n that makes an angle α with y_m :

$$\alpha(y_m, x_n) = \arccos \frac{y_m \cdot x_n}{|y_m| \times |x_n|} \in [0, \pi]. \quad (4)$$

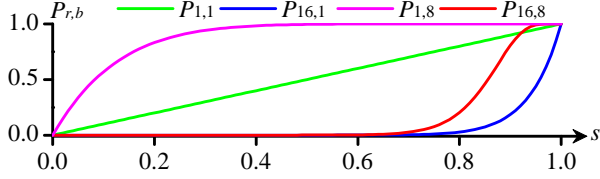


Figure 3. The $P_{r,b}$ - s curve. The (r, b) values of green, blue, magenta and red curves are $(1, 1)$, $(16, 1)$, $(1, 8)$ and $(16, 8)$ respectively. Best viewed in color.

The probability that the i -th bit of $\text{bin}(\mathbf{h}_{j,\mathbf{y}_m})$ and $\text{bin}(\mathbf{h}_{j,\mathbf{x}_n})$ has the equal value is:

$$\mathcal{P}(\text{bin}(\mathbf{h}_{j,\mathbf{y}_m})^{<i>} \equiv \text{bin}(\mathbf{h}_{j,\mathbf{x}_n})^{<i>}) = \frac{\pi - \alpha}{\pi}. \quad (5)$$

Therefore, in D_j , the probability of \mathbf{x}_n being the similar candidate of \mathbf{y}_m (*i.e.* the two binary codes being identical) is:

$$\mathcal{P}(\text{bin}(\mathbf{h}_{j,\mathbf{y}_m}) \equiv \text{bin}(\mathbf{h}_{j,\mathbf{x}_n})) = \left(\frac{\pi - \alpha}{\pi}\right)^r. \quad (6)$$

Considering b hash tables, we take \mathbf{x}_n as a similar candidate of \mathbf{y}_m if there is at least a table that meets the requirement of $\text{bin}(\mathbf{h}_{j,\mathbf{y}_m}) \equiv \text{bin}(\mathbf{h}_{j,\mathbf{x}_n})$, $j \in \{1, \dots, b\}$. Its probability $\mathcal{P}_{r,b}$ is:

$$\mathcal{P}_{r,b}(\alpha) = 1 - \left(1 - \left(\frac{\pi - \alpha}{\pi}\right)^r\right)^b. \quad (7)$$

We use $s = (\pi - \alpha)/\pi$ to denote the similarity of \mathbf{y}_m and \mathbf{x}_n . The $\mathcal{P}_{r,b}$ - s curves of four specific (r, b) values are shown in Fig. 3, where $(r, b) = \{(1, 1), (16, 1), (1, 8), (16, 8)\}$. In the curves for $b > 1$ and $r > 1$, the similarity threshold corresponding to the steepest rise, determines whether \mathbf{y}_m and \mathbf{x}_n are similar or not. An approximation to the threshold [18] is:

$$\hat{s}(r, b) = \left(\frac{1}{b}\right)^{\frac{1}{r}}. \quad (8)$$

Therefore, we can change the similarity threshold \hat{s} by changing the length of hash codes r and the number of hash layers b . If the similarity between \mathbf{y}_m and \mathbf{x}_n is smaller than \hat{s} , \mathbf{x}_n can hardly become a similar candidate of \mathbf{y}_m . Otherwise, it can become the similar candidate with a high probability.

In a vanilla locality-sensitive hashing, we can find all the similar candidates of \mathbf{y}_m in D_1, \dots, D_b and compute the distances between the original training features and \mathbf{y}_m . However, for further reducing computation cost, we directly compute the average distance between $\mathbf{h}_{j,\mathbf{y}_m}$ and the hash codes with the same key $\text{bin}(\mathbf{h}_{j,\mathbf{y}_m})$ in D_j for all $j \in \{1, \dots, b\}$. If $\text{bin}(\mathbf{h}_{j,\mathbf{y}_m})$ is not in D_j , the distance is assigned with a large value. Finally, the minimum distance among all hash tables is taken as the anomaly score for \mathbf{y}_m .

4. Experiments

4.1. Datasets and Setups

4.1.1 Datasets

We evaluate our method on three benchmark datasets and compare the performance with the state of the art.

Avenue. The CUHK Avenue dataset [23] consists of 16 training and 21 testing videos of a single scene. There are 47 abnormal events in the testing videos, such as loitering, wrong direction, and throwing stuff. The resolution of each video is 360×640 pixels.

ShanghaiTech. The ShanghaiTech (*abbr.* ST) dataset [24] contains 330 training and 107 testing videos of 13 scenes. Examples of anomalous events are riding bikes, fighting and vehicles. The resolution of each video is 480×856 pixels. It is the largest dataset among existing benchmarks for video anomaly detection.

Corridor. The IITB Corridor dataset [36] contains 208 training and 150 testing videos of a single scene. Anomalous events include protest, hiding and playing with ball. The resolution of each video is 1920×1080 pixels. It is a new and large benchmark for video anomaly detection.

4.1.2 Evaluation Metrics

The area under curve (AUC) is the most commonly used evaluation metric for video anomaly detection in frame-level. It is computed by the area under the receiver operating characteristic curve with varying thresholds for anomaly scores. A higher value indicates a better performance.

Following the protocol of [11], we evaluate the performance with two clearly defined frame-level AUCs as metrics: 1) macro-averaged AUC (*abbr.* macro-AUC), which first computes the frame-level AUC for each video, then averages the resulting AUCs of videos, and 2) micro-averaged AUC (*abbr.* micro-AUC), which first concatenates frame-level scores of all videos and then computes the AUC. For a fair comparison, the results of different methods are reported under these two evaluation metrics and are compared following the same protocol. In our ablation studies, we use the macro-AUC for evaluation.

4.1.3 Implementation Details

We use the SlowFast network [8] pre-trained on Kinetics-400 dataset [3] to extract features [6]. Training snippets are sampled from random starting positions in videos. Every snippet consists of $T = 32$ frames with the sampling rate $s = 1$. The sampling offset Δt is a random integer in the range of -150 and 150 . All the frames are scaled to 256×256 pixels before fed into the network. We use $b = 8$ hash layers, each of which outputs an $r = 32$ -bit hash code. On ShanghaiTech and Corridor datasets, the length of the

Table 1. Quantitative comparison with state-of-the-art methods for anomaly detection. Numbers in bold: the best performance; * (also in gray text): object-level methods; †: our re-implementations; ‡: results from other papers (no official implementations).

	Year	Method	Avenue	ST	Corridor
Micro-AUC	2018	FFP [21]	85.1	72.8	64.7‡
	2019	AMC [28]	86.9	-	-
		LSA [1]	-	72.5	-
		MPED-RNN [27]	-	73.4	64.3‡
		MemAE [12]	83.3	71.2	-
	2020	PoseCVAE [17]	82.1	74.9	67.3
		MNAD [30]	88.5	70.5	-
		MNAD [30] †	86.9	67.5	68.1
		GEPC [26]	-	76.1	-
		MTP [36]	82.9	76.0	67.1
		CDDA [4]	86.0	73.3	-
		2021	AMMC-Net [2]	86.6	73.7
	HF ² -VAD [22] *		91.1	76.2	-
	MPN [25]		89.5	73.8	-
MPN [25] †	83.9		73.0	69.2	
Ours	LSH	86.5	72.1	73.4	
	LLSH	87.4	77.6	73.5	
Macro-AUC	2019	OADA [15] *	90.4	84.9	-
	2020	MNAD [30] †	80.1	81.7	68.4
	2021	MPN [25] †	81.5	80.2	66.1
		MTL [10]	86.9	83.5	-
	Ours	LSH	86.3	80.5	73.8
LLSH		88.6	85.9	74.2	

queue for each dataset is $l = 8192$, and the batch size is 256. On Avenue dataset, l is set to 2048 and the batch size is 32. The models are trained with a learning rate of 0.001 for 60, 60 and 10 iterations on Avenue, ShanghaiTech and Corridor datasets, respectively. The momentum coefficient m for θ_k is set to 0.999, and the temperature τ in the *InfNCE* loss is 0.2. Our experiments are conducted with four Nvidia RTX-2080Ti GPUs using PyTorch [31]. We follow the previous works [10, 15] to apply a Gaussian filter to temporally smooth the anomaly scores.

4.2. Comparison with the state of the art

We compare our methods using both micro-AUC and macro-AUC evaluation protocols with the state of the art for video anomaly detection on Avenue [23], ShanghaiTech [24] and Corridor [36] datasets, whose results can be seen in Tab. 1. We re-implement MNAD [30] and MPN [25] methods on the three datasets with the help of their official codes,

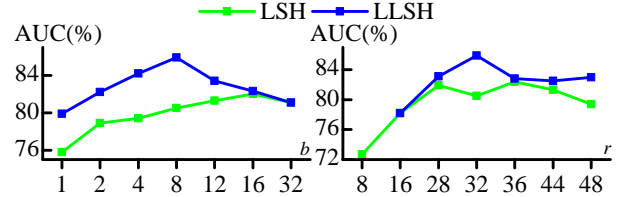


Figure 4. Results of different numbers of hash layers b and different lengths of hash codes r on ST dataset in macro-AUC metric.

which are marked with †. Rodrigues *et al.* [36] have implemented FFP [21] and MPED-RNN [27] on Corridor dataset, so we just report their results, which are marked with ‡. HF²-VAD [22] and OADA [15] are two object-level methods, which are marked with * and in gray text. It should be noted that a comparison between object-level methods and frame-level methods are not fair, for the reason that some anomalies (*e.g.* bikes, skateboards and vehicles) can be recognized by object detectors. Therefore, we only report the frame-level AUC results of MTL [10], and do not take HF²-VAD and OADA into account for comparisons of AUC. Our LSH does not have the training phase. Its parameters are just randomly initialized. LLSH is trained as we introduced in our Method Section.

From the table, we observe three things:

(1) A simple LSH method can achieve good performance in VAD. We can see that our LSH method can surpass several recent methods, such as CDDA [4], MTP [36], PoseCVAE [17], MemAE [12] and FFP [21].

(2) The performance of LLSH is significantly better than LSH, which demonstrates the effectiveness of making the parameters of LSH learnable. The intra-class variations of ShanghaiTech are much larger than Avenue and Corridor datasets since it has 13 different scenes. However, compared with LSH, the improvement of LLSH on that dataset is the largest, indicating that the process of learning improves the adaptability of LSH. Due to the limitation of the input size of the pre-trained CNN, large-scale reduction of the high resolution frames is probably the reason of small improvement on Corridor dataset.

(3) Our proposed LLSH method achieves the best results on the two large-scale datasets, *i.e.*, ShanghaiTech and Corridor in both micro-AUC and macro-AUC evaluation protocols. Its performance on Avenue dataset is also the best in macro-AUC metric, and the third best in micro-AUC metric among frame-level methods. On ShanghaiTech dataset, LLSH outperforms recent memory-augmented prediction methods [2, 12, 25, 30] by 4% ~ 7%. As a frame-level method, it even outperforms object-level methods [15, 22] in both metrics consistently. The outstanding performance demonstrates the superiority of our LLSH.

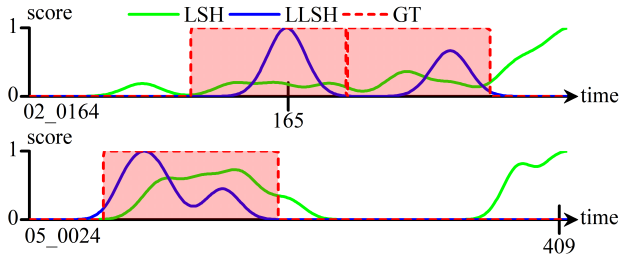


Figure 5. Anomaly score curves of LSH and LLSH on "02_0164" and "05_0024" videos from ST dataset. GT stands for groundtruth. A higher score means a higher probability of anomaly.

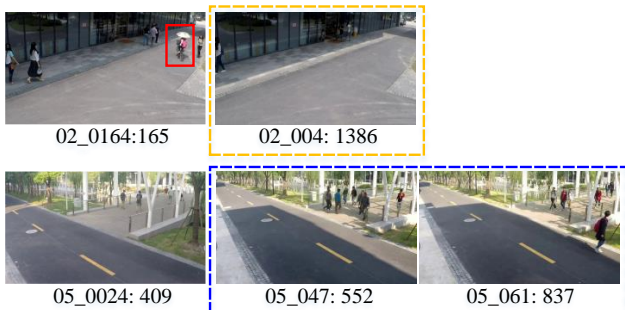


Figure 6. Query snippets (in the first column) and their similar candidate snippets found by LSH (in the orange dashed box) and LLSH (in the blue dashed box). The region in red box represents anomalous region.

4.3. Ablation Study

To study the effects of the number of hash layers b and the length of hash codes r , we perform ablation experiments for the two hyper-parameters on ShanghaiTech dataset. In the study of b , we empirically set r to 32, and in the study of r , b is empirically set to 8. Their results in macro-AUC metric are shown in Fig. 4.

With the increment of b , AUC increases first but then decreases, whose trend resembles that of r . Eq. (8) explains the reason of this phenomenon. As r is fixed, increment of b makes the similarity threshold decline. As a result, dissimilar hash codes are put in the same bucket, causing high false positive rate. As b is fixed, increment of r makes the similarity threshold rise, causing low true positive rate since similar hash codes cannot be put in the same bucket. A way to improve accuracy is increasing b and r simultaneously. However, the cost of computation also increases linearly as one of b and r increases. In our experiments, $b = 8$ and $r = 32$ is a proper setting for our model and does not bring much computation cost.

4.4. Visualization

We visualize two samples from ShanghaiTech dataset to qualitatively analyze how LLSH improves the accuracy for video anomaly detection compared with LSH. The anomaly score curves of LSH and LLSH methods on "02_0164" and "05_0024" videos from ShanghaiTech dataset are shown in Fig. 5. After the process of learning hashing, the AUC on "02_0164" rises from 64.1% (LSH) to 93.7% (LLSH), and rises from 80.2% (LSH) to 99.5% (LLSH) on "05_0024". From the curves we can see that LLSH can increase anomaly scores for anomalous frames and decrease anomaly scores for normal frames, hence improving the accuracy for video anomaly detection.

We take two query snippets which are centered at the 165-th frame of "02_0164" and the 409-th frame of "05_0024" as examples, to visualize how LLSH modifies anomaly scores. For simplicity, we use the center frame to represent a snippet. In the first row of Fig. 6, the snippet in orange dashed box is the only similar candidate found by LSH. The cosine similarity between the features of it and the corresponding query snippet is 0.8786, generating an anomaly score of 0.1756. However, the 165-th frame of "02_0164" is anomalous, which expects a high score. The LLSH method does not find any similar candidates in all the hash tables, thus generating a high score of 0.9965. The 409-th frame of "05_0024" is normal and expects a low score. However, LSH finds no similar candidate and hence generates a high score of 0.9719. In contrast, LLSH finds a total of 9 similar candidates from 3 videos in the nearest bucket. Two of the similar snippets are show in the second row of Fig. 6 in blue dashed box. The average cosine similarity between this query snippet and those 9 similar candidates is 0.8880, according to which LLSH generates a low anomaly score of 0.0001. From the above two examples, we can see that compared with LSH, LLSH can eliminate wrong similar candidates for anomalous queries and find correct similar candidates for normal queries. Therefore, LLSH improves the accuracy for video anomaly detection.

4.5. Efficiency

We conduct a series of experiments using KNN and K-means [32] methods for video anomaly detection, and select the models with high AUC to compare with our proposed methods in performance (macro-AUC), computation cost in the testing phase (number of multiplications) and model size (disk usage). For a testing feature, KNN uses the average distance of the K nearest training features as the anomaly score. K-means adopts the nearest distance between the testing feature and the K cluster centers as the anomaly score. Moreover, we propose a light version of LLSH (light-LLSH), which calculates the mean vector of each bucket in the index stage, *i.e.*, every bucket only contains a mean vector. Comparisons on ShanghaiTech dataset

Table 2. Comparisons of different methods in performance, computation cost and model size on ShanghaiTech dataset. $d=9216$: dimension of feature; $N=792855$, $M=112422$: numbers of training and testing features; t : the maximum iterations; n : number of training hash codes to calculate distance with testing hash codes in query stage; m : number of training hash codes to calculate mean vectors in index stage.

Parameters	KNN	K-means		LSH	LLSH	light-LLSH
	$K=1024$	$t=300$		$b=8, r=32,$ $n=38150830$	$b=8, r=32,$ $n=209872075$	$b=8, r=32, n=490433,$ $m=5650569$
macro-AUC	85.6%	84.1%	83.3%	80.5%	85.9%	85.7%
Number of multiplications	dNM 821.5 Tera	$dKNt + dKM$ 2245.8 Tera / 70.2 Tera		$drb(M + N) + rn$ 2.1 Tera	$drb(M + N) + rn$ 5.5 Giga more than LSH	$drb(M + N) + 2rm + rn$ 0.8 Giga less than LSH
Disk usage	28 GB	111 MB	6.4 MB	1190 MB	993 MB	316 MB

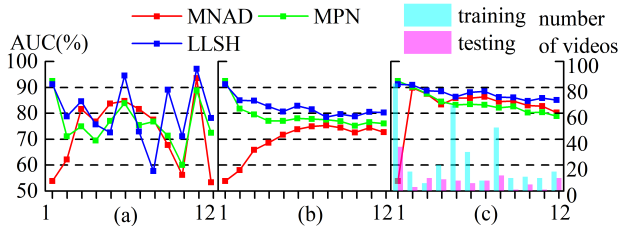


Figure 7. Results (macro-AUC) of MNAD, MPN and LLSH under three circumstances, and video numbers in each scene.

are shown in Tab. 2. It can be seen that: (1) Simple KNN and K-means methods can achieve good performance in anomaly detection. (2) Our LSH, LLSH and light-LLSH require much less computation cost than KNN and K-means, demonstrating the efficiency of our methods. Specifically, the computation cost of LLSH is only 0.26% of KNN and 3.00% of K-means ($K=32$). (3) The proposed light-LLSH has a slightly worse performance but much less computation cost and model size than LLSH. Although K-means has the smallest model size, its performance is significantly worse than light-LLSH and causes large computation cost. Overall, our light-LLSH makes the best trade-off among performance, computation cost and model size.

4.6. Adaptability

ShanghaiTech is the most challenging dataset since it has large intra-class variations and imbalanced distribution. Therefore, we use it to study the adaptability of different methods. We compare MNAD [30], MPN [25] and our LLSH under three circumstances: (a) training and testing models in each single scene, (b) computing average result of the first N scenes obtained in (a), and (c) training and testing models in the first N scenes. Although there are 13 scenes in the training data, there are 12 scenes in the testing data. Hence we use the 12 common scenes in the experiments, *i.e.*, $N \in \{1, 2, \dots, 12\}$. Fig. 7 shows the results under these three circumstances and numbers of training/testing videos in each scene. From the results in (a) and (b) we can see that LLSH outperforms MNAD and MPN in most scenes consistently. In the 8-th scene, jogging in the

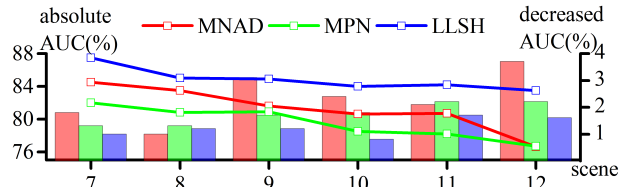


Figure 8. Results (macro-AUC) of MNAD, MPN and LLSH for newly added scenes on ST dataset. The lines/bars are absolute/decreased AUCs on the first 7, 8, \dots , 12 scenes, where a higher value means better/worse respectively.

crowd causes occlusion and breaks the continuity of motion, thus our frozen pre-trained CNN cannot extract discriminative representations for some snippets. For this reason, LLSH gets a lower result in this scene. The results of (c) demonstrates the super adaptability of LLSH since it can always achieve the best performance with the increment of new scenes, even if video numbers change largely in different scenes. Besides, comparing the results of (b) and (c), we find that all the three methods can benefit from training in multiple scenes. That is to say, normal information between different scenes can conduce to complement each other.

4.7. Scalability

A model with strong scalability has more practical application value. Therefore, we compare the scalability of MNAD [30], MPN [25] and the proposed LLSH for newly added scenes. For each model, we train it on the first 6 scenes of ShanghaiTech dataset, and directly test it on the first 7, 8, \dots , 12 scenes. The results are shown in Fig. 8, where absolute AUCs are plotted in lines, and decreased AUCs compared with training with all the scenes together are plotted in bars. LLSH consistently achieves the best performance in absolute AUC for different numbers of newly added scenes. In addition, it nearly always has the least decline of performance, which indicates its superior of scalability. Our proposed LLSH has the advantages of both learnable models and non-learnable algorithms, making it adaptive and also retaining its scalability.

5. Conclusion

In this paper, we have proposed a novel learnable locality-sensitive hashing (LLSH), which can take full advantage of the knowledge of normal data efficiently and flexibly, to distinguish anomalies from normal events. It implements LSH as a parametric network and trains end-to-end in a contrastive learning framework. Extensive experiments have shown that LLSH is superior in efficiency, adaptability and scalability, achieving new state of the art on VAD benchmarks.

References

- [1] Davide Abati, Angelo Porrello, Simone Calderara, and Rita Cucchiara. Latent space autoregression for novelty detection. In *CVPR*, 2019. 1, 6
- [2] Ruichu Cai, Hao Zhang, Wen Liu, Shenghua Gao, and Zhifeng Hao. Appearance-Motion Memory Consistency Network for Video Anomaly Detection. *AAAI*, 35(2):938–946, 2021. 1, 6
- [3] Joao Carreira and Andrew Zisserman. Quo Vadis, Action Recognition? A New Model and the Kinetics Dataset. In *CVPR*, pages 4724–4733, 2017. 5
- [4] Yunpeng Chang, Zhigang Tu, Wei Xie, and Junsong Yuan. Clustering Driven Deep Autoencoder for Video Anomaly Detection. In *ECCV*, volume 12360, pages 329–345. Springer, 2020. 1, 2, 6
- [5] Ting Chen, Simon Kornblith, Mohammad Norouzi, and Geoffrey Hinton. A simple framework for contrastive learning of visual representations. In *Proceedings of the 37th International Conference on Machine Learning*, volume 119, pages 1597–1607, 2020. 3
- [6] Haoqi Fan, Yanghao Li, Bo Xiong, Wan-Yen Lo, and Christoph Feichtenhofer. Pyslowfast. <https://github.com/facebookresearch/slowfast>, 2020. 5
- [7] Yaxiang Fan, Gongjian Wen, Deren Li, Shaohua Qiu, Martin D. Levine, and Fei Xiao. Video anomaly detection and localization via Gaussian Mixture Fully Convolutional Variational Autoencoder. *Computer Vision and Image Understanding*, 195:102920, 2020. 1
- [8] Christoph Feichtenhofer, Haoqi Fan, Jitendra Malik, and Kaiming He. SlowFast Networks for Video Recognition. In *ICCV*, pages 6201–6210, 2019. 5
- [9] Christoph Feichtenhofer, Haoqi Fan, Bo Xiong, Ross Girshick, and Kaiming He. A Large-Scale Study on Unsupervised Spatiotemporal Representation Learning. In *CVPR*, pages 3299–3309, 2021. 3
- [10] Mariana-Iuliana Georgescu, Antonio Barbalau, Radu Tudor Ionescu, Fahad Shahbaz Khan, Marius Popescu, and Mubarak Shah. Anomaly Detection in Video via Self-Supervised and Multi-Task Learning. In *CVPR*, pages 12742–12752, 2021. 1, 6
- [11] Mariana Iuliana Georgescu, Radu Ionescu, Fahad Shahbaz Khan, Marius Popescu, and Mubarak Shah. A Background-Agnostic Framework with Adversarial Training for Abnormal Event Detection in Video. *IEEE TPAMI*, pages 1–1, 2021. 5
- [12] Dong Gong, Lingqiao Liu, Vuong Le, Budhaditya Saha, Moussa Reda Mansour, Svetha Venkatesh, and Anton Van Den Hengel. Memorizing Normality to Detect Anomaly: Memory-Augmented Deep Autoencoder for Unsupervised Anomaly Detection. In *ICCV*, pages 1705–1714, 2019. 1, 6
- [13] Mahmudul Hasan, Jonghyun Choi, Jan Neumann, Amit K. Roy-Chowdhury, and Larry S. Davis. Learning temporal regularity in video sequences. In *CVPR*, 2016. 1
- [14] Kaiming He, Haoqi Fan, Yuxin Wu, Saining Xie, and Ross Girshick. Momentum Contrast for Unsupervised Visual Representation Learning. In *CVPR*, pages 9726–9735, 2020. 2, 3
- [15] Radu Tudor Ionescu, Fahad Shahbaz Khan, Mariana-Iuliana Georgescu, and Ling Shao. Object-Centric Auto-Encoders and Dummy Anomalies for Abnormal Event Detection in Video. In *CVPR*, pages 7834–7843, 2019. 1, 2, 6
- [16] Radu Tudor Ionescu, Sorina Smeureanu, Marius Popescu, and Bogdan Alexe. Detecting Abnormal Events in Video Using Narrowed Normality Clusters. In *IEEE Winter Conference on Applications of Computer Vision (WACV)*, pages 1951–1960, 2019. 1, 2
- [17] Yashswi Jain, Ashvini Kumar Sharma, Rajbabu Velmurugan, and Biplab Banerjee. PoseCVAE: Anomalous Human Activity Detection. In *ICPR*, pages 2927–2934, 2021. 1, 6
- [18] Jurij Leskovec, Anand Rajaraman, and Jeffrey D. Ullman. *Mining of Massive Datasets*. Cambridge University Press, third edition edition, 2020. 5
- [19] Kevin Lin, Huei-Fang Yang, Jen-Hao Hsiao, and Chu-Song Chen. Deep learning of binary hash codes for fast image retrieval. In *CVPR*, pages 27–35, 2015. 2
- [20] Haomiao Liu, Ruiping Wang, Shiguang Shan, and Xilin Chen. Deep supervised hashing for fast image retrieval. In *CVPR*, 2016. 2
- [21] Wen Liu, Weixin Luo, Dongze Lian, and Shenghua Gao. Future Frame Prediction for Anomaly Detection - A New Baseline. In *CVPR*, pages 6536–6545, 2018. 1, 6
- [22] Zhian Liu, Yongwei Nie, Chengjiang Long, Qing Zhang, and Guiqing Li. A hybrid video anomaly detection framework via memory-augmented flow reconstruction and flow-guided frame prediction. In *ICCV*, pages 13588–13597, 2021. 1, 6
- [23] Cewu Lu, Jianping Shi, and Jiaya Jia. Abnormal event detection at 150 FPS in MATLAB. In *ICCV*, 2013. 1, 2, 5, 6
- [24] Weixin Luo, Wen Liu, and Shenghua Gao. A Revisit of Sparse Coding Based Anomaly Detection in Stacked RNN Framework. In *ICCV*, pages 341–349, 2017. 1, 2, 5, 6
- [25] Hui Lv, Chen Chen, Zhen Cui, Chunyan Xu, Yong Li, and Jian Yang. Learning normal dynamics in videos with meta prototype network. In *CVPR*, pages 15425–15434, 2021. 1, 6, 8
- [26] Amir Markovitz, Gilad Sharir, Itamar Friedman, Lih Zelnik-Manor, and Shai Avidan. Graph Embedded Pose Clustering for Anomaly Detection. In *CVPR*, pages 10536–10544, 2020. 1, 2, 6
- [27] Romero Morais, Vuong Le, Truyen Tran, Budhaditya Saha, Moussa Mansour, and Svetha Venkatesh. Learning Reg-

- ularity in Skeleton Trajectories for Anomaly Detection in Videos. In *CVPR*, pages 11988–11996, 2019. 1, 6
- [28] Trong Nguyen Nguyen and Jean Meunier. Anomaly Detection in Video Sequence With Appearance-Motion Correspondence. In *ICCV*, pages 1273–1283, 2019. 1, 6
- [29] Viet-Anh Nguyen and Minh N. Do. Deep learning based supervised hashing for efficient image retrieval. In *ICME*, pages 1–6, 2016. 2
- [30] Hyunjong Park, Jongyoun Noh, and Bumsub Ham. Learning Memory-Guided Normality for Anomaly Detection. In *CVPR*, pages 14360–14369, 2020. 1, 6, 8
- [31] Adam Paszke, Sam Gross, Soumith Chintala, Gregory Chanan, Edward Yang, Zachary DeVito, Zeming Lin, Alban Desmaison, Luca Antiga, and Adam Lerer. Automatic differentiation in PyTorch. page 4, 2017. 6
- [32] F. Pedregosa, G. Varoquaux, A. Gramfort, V. Michel, B. Thirion, O. Grisel, M. Blondel, P. Prettenhofer, R. Weiss, V. Dubourg, J. Vanderplas, A. Passos, D. Cournapeau, M. Brucher, M. Perrot, and E. Duchesnay. Scikit-learn: Machine learning in Python. *Journal of Machine Learning Research*, 12:2825–2830, 2011. 7
- [33] Bharathkumar Ramachandra and Michael Jones. Street Scene: A new dataset and evaluation protocol for video anomaly detection. In *IEEE Winter Conference on Applications of Computer Vision (WACV)*, 2020. 1, 2
- [34] Bharathkumar Ramachandra, Michael Jones, and Ranga Raju Vatsavai. A Survey of Single-Scene Video Anomaly Detection. *IEEE TPAMI*, pages 1–1, 2020. 1
- [35] Bharathkumar Ramachandra, Michael J. Jones, and Ranga Raju Vatsavai. Learning a distance function with a Siamese network to localize anomalies in videos. In *IEEE Winter Conference on Applications of Computer Vision (WACV)*, pages 2587–2596, 2020. 1, 2
- [36] Royston Rodrigues, Neha Bhargava, Rajbabu Velmurugan, and Subhasis Chaudhuri. Multi-timescale Trajectory Prediction for Abnormal Human Activity Detection. In *IEEE Winter Conference on Applications of Computer Vision (WACV)*, pages 2615–2623, 2020. 1, 2, 5, 6
- [37] Sorina Smeureanu, Radu Tudor Ionescu, Marius Popescu, and Bogdan Alexe. Deep Appearance Features for Abnormal Behavior Detection in Video. In *Image Analysis and Processing - ICIAP*, volume 10485, pages 779–789. Springer, 2017. 2
- [38] Hanh Tran and David C. Hogg. Anomaly Detection using a Convolutional Winner-Take-All Autoencoder. In *BMVC*, 2017. 2
- [39] Aaron van den Oord, Yazhe Li, and Oriol Vinyals. Representation learning with contrastive predictive coding. *arXiv preprint arXiv:1807.03748*, 2018. 3
- [40] Ziming Wang, Yuexian Zou, and Zeming Zhang. Cluster Attention Contrast for Video Anomaly Detection. In *ACM MM*, pages 2463–2471, 2020. 1, 2, 3
- [41] Dan Xu, Elisa Ricci, Yan Yan, Jingkuan Song, and Nicu Sebe. Learning deep representations of appearance and motion for anomalous event detection. In *BMVC*, pages 8.1–8.12, 2015. 2